CHEMISTRY OF MATERIALS

Article

Cite This: Chem. Mater. 2020, 32, 374−380

pubs.acs.org/cm

# Bulk Assemblies of Lead Bromide Trimer Clusters with Geometry-Dependent Photophysical Properties

Sujin Lee,[†] Chenkun Zhou,[‡] Jennifer Neu,[§] Drake Beery,[†] Ashley Arcidiacono,[†] Maya Chaaban,[†] Haoran Lin,[†] Alyssa Gaiser,[†] Banghao Chen,[†] Thomas E. Albrecht-Schmitt,[†] Theo Siegrist,[‡,§] and Biwu Ma*[,†,‡]

[†]Department of Chemistry and Biochemistry, Florida State University, Tallahassee, Florida 32306, United States

[‡]Department of Chemical and Biomedical Engineering, FAMU-FSU College of Engineering, Tallahassee, Florida 32310, United States

[§]National High Magnetic Field Laboratory, Florida State University, Tallahassee, Florida 32310, United States

Supporting Information

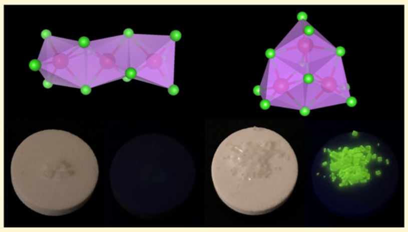

**ABSTRACT:** Single crystalline bulk assemblies of metal halide clusters show great potential as highly efficient light emitters with tunable photophysical properties. However, synthetic control of the geometry of the clusters in a rational manner has not been well established, and the relationships between the photophysical properties and structures of this emerging class of zero-dimensional materials are still not well understood. Here, we report the synthesis and characterization of two bulk assemblies of lead bromide clusters, $(bmpy)_6[Pb_3Br_{12}]$ (**T1**) and $(bmpy)_9[ZnBr_4]_2[Pb_3Br_{11}]$ (**T2**) (bmpy: 1-butyl-1-methylpyrrolidinium), which contain metal halide trimer clusters with different geometries. **T1** with chain-shaped $[Pb_3Br_{12}]^{6-}$ clusters is not emissive at room temperature, whereas **T2** with triangle-shaped $[Pb_3Br_{11}]^{5-}$ clusters exhibits yellowish-green emission peaked at 564 nm with a photoluminescence quantum efficiency of 7% at room temperature. Detailed analysis of the structural and photophysical properties show that the photophysical properties and excited-state dynamics of these materials are highly dependent on the geometry of the metal halide clusters.

## INTRODUCTION

Organic metal halide hybrids have received a great deal of attention for their potential applications in various types of optoelectronic devices.[1−5] By choosing appropriate organic and metal halide components, dimensionality control of metal halides at the molecular level from two-dimensional layers[6,7] to one-dimensional chains[8,9] and zero-dimensional (0D) structures[10,11] can be realized. With metal halides isolated from each other by large organic moieties, 0D structures allow single crystals to exhibit the properties of individual metal halide species. Efficient broadband emissions with large Stokes shift have been observed in many 0D organic metal halide hybrids reported to date, owing to pronounced structural distortion upon photoexcitation.[12] Recent studies have shown that metal halides with different geometries can be used to form 0D structures, for instance, octahedral $SnX_6$, pyramidal $SbX_5$, and disphenoidal $SnX_4$, to display distinct photophysical properties.[10,13−19]

Beyond mononuclear metal halide species, metal halide clusters with multiple metal centers can also be present in 0D structures that exhibit highly efficient emissions with remarkable photostability and thermostability. For instance, by controlling the molecular environment of metal halide clusters, bulk assemblies of triangle-shaped $[Pb_3Cl_{11}]^{5-}$ clusters can emit bright blue or green emissions.[16] Another 0D hybrid containing linear chain-shape metal halide trimer clusters was reported to exhibit emission from Pb vacancies.[20] These results suggest bulk assemblies of metal halide clusters could act as promising light emitters with tunable properties. However, the understanding of the relationships between the geometry of clusters and photophysical properties is still very limited.

Here, we report the synthesis and characterization of two single crystalline bulk assemblies of lead bromide trimer clusters, $(bmpy)_6[Pb_3Br_{12}]$ (**T1**) and $(bmpy)_9[ZnBr_4]_2[Pb_3Br_{11}]$ (**T2**) (bmpy: 1-butyl-1-methylpyrrolidinium). Single crystals were grown by carefully optimizing the synthesis conditions. Interestingly, **T1** is not emissive at room temperature, while **T2** emits yellowish-green light peaked at 564 nm with a photoluminescence quantum efficiency (PLQE) of 7%. Temperature-dependent emission spectra were recorded to gain a better understanding of the intrinsic photophysical properties of 0D metal halide clusters. The geometry-dependent photophysical properties of these metal halide clusters suggest that there are a variety of ways to control the properties of bulk assemblies of metal halide clusters.

Received: September 22, 2019
Revised: December 9, 2019
Published: December 11, 2019

DOI: 10.1021/acs.chemmater.9b03893
Chem. Mater. 2020, 32, 374−380

## RESULTS AND DISCUSSION

Two different single crystalline bulk assemblies of lead bromide trimer clusters were prepared via a vapor diffusion method at room temperature. **T1** single crystals were obtained by diffusing diethyl ether into a dimethylformamide (DMF) precursor solution containing lead bromide ($PbBr_2$) and 1-butyl-1-methylpyrrolidinium bromide (bmpyBr). **T2** single crystals were synthesized by diffusing acetone into DMF precursor solution containing $PbBr_2$, (bmpy)Br, and $ZnBr_2$. Both **T1** and **T2** single crystals are colorless and transparent under ambient light. Upon UV (365 nm) excitation, **T1** bulk crystals are not emissive, while **T2** shows yellowish-green emission at room temperature, as shown in Figure 1.

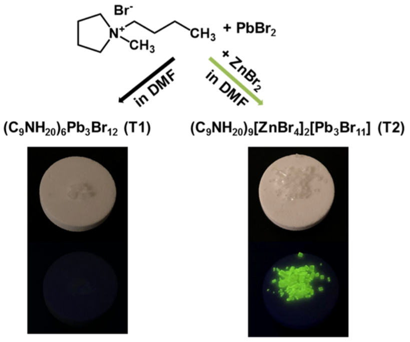

**Figure 1.** Synthetic scheme for the preparation of **T1** and **T2**, and the images of single crystals of **T1** and **T2** under ambient light and UV lamp irradiation (365 nm).

The single crystal X-ray diffraction (SCXRD) characterizations show that **T1** crystallizes in a trigonal space group $R\overline{3}$ and **T2** crystallizes in a hexagonal space group $P6_3$. More detailed structural analysis can be found in the Supporting Information (Tables S1−S3). Figure 2 shows the views of the crystal structures of **T1** and **T2**. In these metal halide clusters, three $PbBr_6$ octahedra form Pb bromide trimers via face-sharing. Interestingly, the shapes of the clusters are different with chain-shaped $[Pb_3Br_{12}]^{6-}$ units found in **T1** and triangle-shaped $[Pb_3Br_{11}]^{5-}$ units found in **T2**. Specifically, an individual $[Pb_3Br_{12}]^{6-}$ cluster in **T1** has two different octahedra forming $[Pb2Br_6{-}Pb1Br_6{-}Pb2Br_6]$ trimers in a linear chain with the angle of Pb2−Pb1−Pb2 at 180°, which is similar to that in $[Pb_3I_{12}]^{6-}$.[9−21] Furthermore, an individual $[Pb_3Br_{11}]^{5-}$ cluster in **T2** has symmetric fused octahedra $[Pb1Br_6{-}Pb1Br_6{-}Pb1Br_6]$ with a near ideal $D_{3h}$ structure. Similar to the previously reported $(C_9NH_{20})_9[ZnCl_4]_2[Pb_3Cl_{11}]$,[16] the wide band gap $[ZnBr_4]^{2-}$ tetrahedra in **T2**, solely acting as anionic spacers, cocrystallize with $[Pb_3Br_{11}]^{5-}$ clusters to stabilize the crystal structure, as depicted in Figure 2D. In addition to the different geometries of Pb bromide clusters, the distortions of $PbBr_6$ octahedra are also very different in the two types of clusters. To better quantify the difference between $[Pb_3Br_{12}]^{6-}$ clusters in **T1** and $[Pb_3Br_{11}]^{5-}$ clusters in **T2**, several parameters were calculated and are summarized in Table 1, including bond length distortion ($\Delta_{oct}$), halide distance deviation (DI(X−X)), octahedral elongation ($\lambda_{oct}$), octahedral angle variance ($\sigma_{oct}^2$), and volume discrepancy ($V$) (see Supporting Information for details). In $[Pb_3Br_{12}]^{6-}$ clusters, Pb1 is coordinated by six Br4 to form a regular octahedron with a bond length distortion $\Delta_{oct} = 0$; Pb2 is bonded to three Br3 and Br4 to form a distorted octahedron with distances of bond length $d_{(Pb2-Br3)} = 2.9192$ and $d_{(Pb2-Br4)} = 3.2433$ Å, with a structural distortion $\Delta_{oct} = 27.7 \times 10^{-4}$. Compared to $Pb2Br_6$ octahedra in **T1**, $Pb1Br_6$ octahedra in **T2** have a different distortion with $\Delta_{oct} = 13.7 \times 10^{-4}$, which is relatively similar to the distortion of other triangle-shaped $[Pb_3Cl_{11}]^{5-}$ clusters ($\Delta_{oct}$ of $(bmpy)_7[PbCl_4][Pb_3Cl_{11}] = 15.9 \times 10^{-4}$ and $\Delta_{oct}$ of $(bmpy)_9[ZnCl_4]_2[Pb_3Cl_{11}] = 16.5 \times 10^{-4}$).[10,11] $^{207}$Pb solid state NMR was also used to characterize the structures of **T1** and **T2** (Figure S1), which clearly shows the different chemical shifts for Pb in two different materials. **T1** exhibits two lead sites at −365.7 and 169.9 ppm and in **T2** only one lead site at 47.5 ppm is observed, as a result of highly symmetric structure of $[Pb_3Br_{11}]^{5-}$. As the geometry and structure distortion could dramatically affect the excited state dynamics of metal halides, distinct photophysical properties are expected for these two materials. The uniformity of **T1** and **T2** single crystals was confirmed by powder XRD (Figure S2), and the compositions of both the single crystals were further confirmed by elemental analysis (Table S4). The high thermostability of **T1** and **T2** with decomposition temperature over 300 °C was observed using thermogravimetry analysis (TGA) analysis (Figure S3).

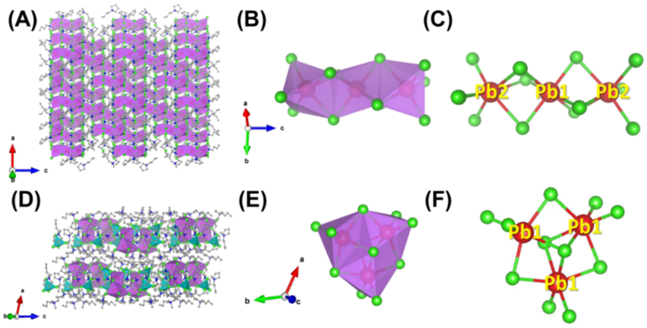

**Figure 2.** (A) View of the single crystal structure of $(bmpy)_6[Pb_3Br_{12}]$ (red spheres, lead atoms; green spheres, bromide atoms; purple, polyhedrons; $[Pb_3Br_{12}]^{6-}$; hydrogen atoms were hidden for clarity). (B) View of individual metal halide trimer clusters $[Pb_3Br_{12}]^{6-}$. (C) Ball-and-stick model of an individual $[Pb_3Br_{12}]^{6-}$ cluster. (D) View of the single crystal structure of $(bmpy)_9[ZnBr_4]_2[Pb_3Br_{11}]$ (deep-blue tetrahedrons, $[ZnBr_4]^{2-}$). (E) View of individual metal halide trimer clusters $[Pb_3Br_{11}]^{5-}$. (F) Ball-and-stick model of an individual $[Pb_3Br_{11}]^{5-}$ cluster.

The photophysical properties of **T1** and **T2** were characterized using UV−vis absorption and emission spectrometers, and time-resolved PL spectrometer (summaries in Table 2). Figure 3A shows the absorption and emission spectra of two single crystals. **T1** is almost nonemissive at room temperature. **T2** exhibits yellowish-green emission peaked at 564 nm with a Stokes shift of 185 nm, a full width at half-maximum (fwhm) of 68 nm, and a PLQE of ∼7%. The excitation energy of **T2** (3.27 eV) (Figure S4) is significantly lower than the band gap of organic cations (∼4 eV) and $ZnBr_4^{2-}$ (∼5 eV), and the yellowish-green emission of **T2** is likely attributed to $Pb_3Br_{11}^{5-}$ clusters.[22] To ensure the intrinsic nature of this emission, we have measured the dependence of emission intensity on the excitation power density at room temperature. As shown in Figure S5, the emission intensity of **T2** exhibits a linear dependence on the excitation power density, suggesting that the emission is its intrinsic property rather than from defects. The Commission Internationale de I'Eclairage (CIE) chromaticity coordinates of **T2** emission was determined to be (0.40, 0.53) at room temperature, as shown

Table 1. Structural Distortion Comparisons of Selected Pb Octahedra in T1 and T2[a]

| | $(bmpy)_6[Pb_3Br_{12}]$ (**T1**) | | | | $(bmpy)_9[ZnBr_4]_2[Pb_3Br_{11}]$ (**T2**) | | | |
|---|---|---|---|---|---|---|---|---|
| | Pb1 | $Pb2^1$ | $Pb2^2$ | avg. | $Pb1^1$ | $Pb1^2$ | $Pb1^3$ | avg. |
| $d_{avg}$ | 3.014 | 3.081 | 3.081 | 3.059 | 3.026 | 3.026 | 3.026 | 3.026 |
| $\Delta_{oct} \times 10^4$ | 0 | 27.7 | 27.7 | 18.4 | 13.7 | 13.7 | 13.7 | 13.7 |
| DI(X−X) | 0.020 | 0.051 | 0.051 | 0.041 | 0.045 | 0.045 | 0.045 | 0.045 |
| $\lambda_{oct}$ | 1.002 | 1.028 | 1.028 | 1.019 | 1.020 | 1.020 | 1.020 | 1.020 |
| $\sigma_{oct}^2$ | 5.756 | 85.436 | 85.436 | 58.876 | 67.116 | 67.116 | 67.116 | 67.116 |
| $V$ (%) | 0.176 | 2.394 | 2.394 | 1.655 | 0.794 | 0.794 | 0.794 | 0.794 |

[a] Bond length distortion ($\Delta_{oct}$), halide distance deviation (DI(X−X)), octahedral elongation ($\lambda_{oct}$), octahedral angle variance ($\sigma_{oct}^2$), and volume discrepancy ($V$).

Table 2. Summary of Photophysical Properties of T1 and T2[a]

| material | $\lambda_{exc}$ (nm) | $\lambda_{em}$ (nm) | fwhm (nm) | Stokes shift (nm) | Φ (%) | $\tau_{av}$ ($\mu$s) |
|---|---|---|---|---|---|---|
| **T1** | N/A (345) | N/A (501, 564) | N/A (135) | N/A (156) | N/A | N/A (18[b], 44[c]) |
| **T2** | 379 (345) | 564 (474, 580) | 68 (61) | 185 (129) | 7 | 0.036 (25[d], 12[e]) |

[a] Data in parentheses were for 77 K. [b] PL decay profiles at 77 K were measured at 500 nm [c] PL decay profiles at 77 K were measured at 552 nm. [d] PL decay profiles at 77 K were measured at 474 nm. [e] PL decay profiles at 77 K were measured at 580 nm.

in Figure 3B. As compared to previously reported $(bmpy)_9[ZnCl_4]_2[Pb_3Cl_{11}]$, a red shift of 52 nm for the peak emission was achieved for **T2**, as a result of halide substitution.[16] The luminescence of **T2** has a monoexponential decay lifetime of 36 ns (Figure 3C).

The photophysical properties were also investigated at 77 K (Table 2). Interestingly, **T1** has two emission peaks at 501 and 564 nm with decay lifetimes of 18 and 44 $\mu$s, respectively (Figure 4A,B). For **T2**, the emission becomes narrower and the peak blue-shifts to 474 nm with a shoulder at around 580 nm. The decay lifetimes for these two peaks are 25 and 12 $\mu$s, respectively. To better understand the photophysical properties of **T1** and **T2**, temperature-dependent PL spectra were recorded from 80 K to room temperature (Figure 5). It was found that the emissions of both **T1** and **T2** can be described as combinations of two Gaussian shaped emissions with their intensities depending on the temperature. A model is proposed in the next session to describe the potential energy surface. In the case of **T2**, as shown in Figure 5B, the emission peaked at 580 nm gradually decreases with a new emission peaked at high energy region emerging when the temperature decreases,

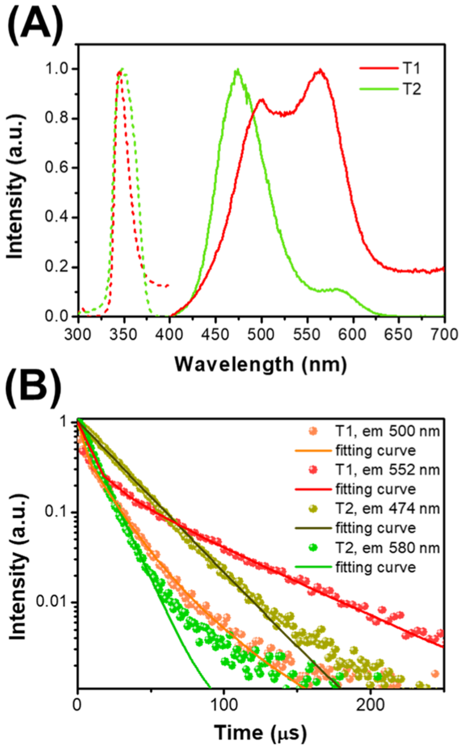

**Figure 4.** (A) Excitation and emission spectra of **T1** and **T2** at 77 K and (B) emission decay of **T1** and **T2** at 77 K.

which is identical to the behavior of the previously reported chloride counterpart $(bmpy)_9[ZnCl_4]_2[Pb_3Cl_{11}]$.[16] The spectra of **T1** with normalization and **T2** without normalization are shown in Figure S6 for reference. At temperatures above room temperature, the shapes of the emission spectra of **T2** do not change, suggesting the same origin of emissions at this temperature region. The thermal stability of **T2** is relatively

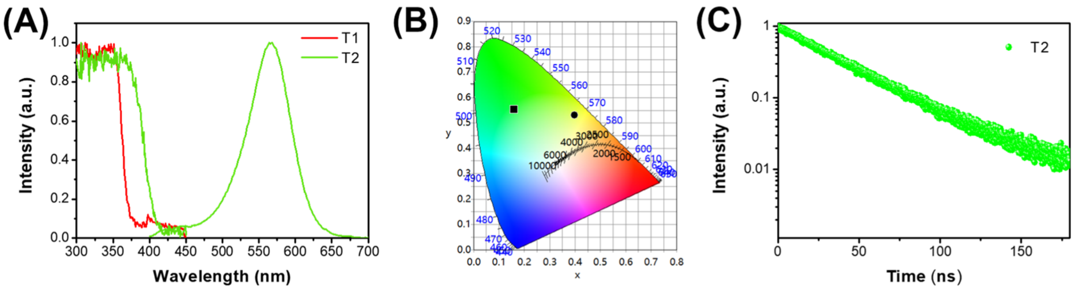

**Figure 3.** (A) Absorption and emission spectra of **T1** and **T2** at room temperature; (B) CIE chromaticity coordinates of the emissions from **T2** (circle) and $(bmpy)_9[ZnCl_4]_2[Pb_3Cl_{11}]$ (square); and (C) emission decay of **T2** at room temperature.

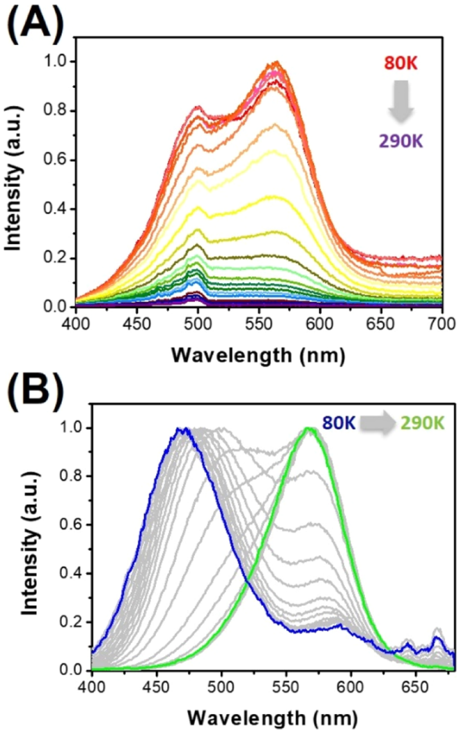

**Figure 5.** Temperature-dependent emission spectra of **T1** (A) and **T2** (B) from 80 K to room temperature (10 K/scan).

good as the emission intensity could fully recover when the temperature returns to room temperature (Figure S7).

We propose possible potential energy surfaces for **T1** and **T2**, as depicted in Figure 6, to explain their different photophysical characteristics. Two excited-state energy minima (ES1 and ES2) coexist on the potential energy surfaces with different energy barriers for **T1** and **T2**, and the energy barriers ($E_a$ from ES1 to ES2 and $E_b$ from ES2 to ES1) between two states strongly depend on the geometry of metal halide clusters. In **T1**, there are two different molecular environments for three Pb in an individual chain-shaped metal halide cluster; therefore, the photo-generated excitons could be localized in both distorted $PbBr_6$ and $Pb2Br_6$ simultaneously (ES1 and ES2) upon photoexcitation. Two energy barriers ($E_a$ and $E_b$) were estimated by analyzing several emission characteristics, with details shown in the Supporting Information (Figure S8). The analysis method is similar to that for dual emitting platinum binuclear complexes with photoinduced structural change.[23] The estimated energy barriers $E_a$ and $E_b$ are close to each other in the order of 0.007 eV (thermal energy at 80 K), which could be overcome by thermal energy, resulting in an equilibrium between ES1 and ES2 in a wide range of temperatures for **T1**. In **T2**, which has the same molecular environment for three Pb in an ideal $D_{3h}$ metal halide cluster, two energy barriers are significantly different, with $E_a$ on the order of 0.025 eV and $E_b$ 0.166 eV higher (see Supporting Information for detailed analysis). These energy barriers could prevent the formation of equilibrium, but afford strongly temperature-dependent emissions, that is, emission mainly from ES1 at 77 K and from ES2 at room temperature, similar to that of $(bmpy)_9[ZnCl_4]_2[Pb_3Cl_{11}]$.[16]

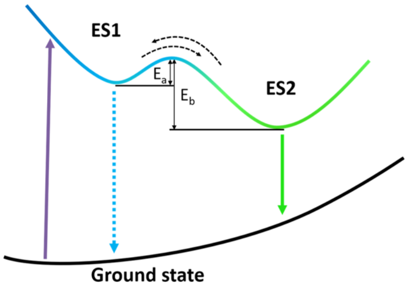

**Figure 6.** Potential energy surfaces and photophysical processes for **T1** and **T2** with two excited-state energy minima (ES1 and ES2); $E_a$ and $E_b$ are the energy barriers.

## ■ CONCLUSIONS

In summary, we have synthesized and characterized two single crystalline bulk assemblies of metal halide clusters, $(bmpy)_6[Pb_3Br_{12}]$ (**T1**) and $(bmpy)_9[ZnBr_4]_2[Pb_3Br_{11}]$ (**T2**), where **T1** contains chain-shaped $[Pb_3Br_{12}]^{6-}$ units and **T2** contains triangle-shaped $[Pb_3Br_{11}]^{5-}$ units. Detailed structural and photophysical studies showed that the photophysical properties of these materials are highly dependent on the geometry of the metal halide clusters. Possible potential energy surfaces for these materials are proposed to explain their different photophysical properties, in which different energy barriers are present between two excited states. Our work advances research in organic metal halide hybrids with synthetic control of the geometry of the metal halide clusters and provides new understanding of the structure−property relationships for this class of materials.

## ■ EXPERIMENTAL SECTION

**Materials.** Lead(II) bromide ($PbBr_2$, 99.999%) was purchased from Sigma-Aldrich. 1-Butyl-1-methylpyrrolidinium bromide ($C_9H_{20}NBr$, >97%) was purchased from TCI. Zinc bromide ($ZnBr_2$, 99.9%) was purchased from Alfa Aesar. DMF (99.8%), acetone (anhydrous, 99.9%), and diethyl ether ($Et_2O$, anhydrous) were purchased from VWR. All reagents and solvents were used without further purification unless otherwise stated.

**Solution Growth of $(bmpy)_6Pb_3Br_{12}$ Single Crystals.** $PbBr_2$ (0.27 mmol) and bmpyBr (2.2 mmol) were mixed and dissolved in DMF to form a clear precursor solution. Bulk crystals were prepared by diffusing diethyl ether into the prepared precursor solution at room temperature overnight. The large colorless crystals were washed with diethyl ether and dried under reduced pressure. The yield was calculated at ∼23%. Anal. Calcd: C, 26.65; H, 4.97; N, 3.45; Br, 39.39. Found: C, 26.89; H, 4.85; N, 3.35; Br, 39.64.

**Solution Growth of $(bmpy)_9[ZnBr_4]_2[Pb_3Br_{11}]$ Single Crystals.** $PbBr_2$ (0.27 mmol), $ZnBr_2$ (0.54 mmol), and bmpyBr (2.2 mmol) were mixed and dissolved in DMF to form a clear precursor solution. Bulk crystals were prepared by diffusing acetone into prepared precursor solution at room temperature overnight. The large colorless crystals were washed with acetone and dried under reduced pressure. The yield was calculated at ∼28%. Anal. Calcd: C, 27.40; H, 5.11; N, 3.55; Br, 42.75. Found: C, 27.66; H, 5.08; N, 3.41; Br, 43.04.

**SCXRD of $(bmpy)_6Pb_3Br_{12}$.** SCXRD data of $(bmpy)_6Pb_3Br_{12}$ were collected using an Oxford-Diffraction Xcalibur-2 CCD diffractometer with graphite-monochromated Mo K$\alpha$ radiation. The crystal was mounted in a Cryoloop under Paratone-N oil and cooled to 100 K with an Oxford-Diffraction Cryojet. A hemisphere of data was collected using $\omega$ scans with 1° frame widths to a resolution of 0.75 Å, equivalent to $2\theta \approx 56°$. Reflections were recorded, indexed, and corrected for absorption using the Oxford-Diffraction CrysAlisPro software,[24] and subsequent structure determination and refinement was carried out using CRYSTALS,[25] employing Superflip[26] to solve the crystal structure. The data allowed for unconstrained refinement of all non-hydrogen atomic positions; hydrogens were geometrically restrained to their associated carbons. The refinement was performed against $F^2$, with anisotropic thermal displacement parameters for all atoms and with isotropic thermal displacement parameters for the hydrogens in the structure. A CIF has been deposited with the CCDC (1895392).

**SCXRD of (bmpy)$_9$[ZnBr$_4$]$_2$[Pb$_3$Br$_{11}$].** SCXRD was used to fully determine the inorganic cage structure and to accurately position the associated organic ligands of (bmpy)$_9$[ZnBr$_4$]$_2$[Pb$_3$Br$_{11}$] within it. Single crystal data were collected using an Oxford-Diffraction Xcalibur-2 CCD diffractometer with graphite-monochromated Mo K$\alpha$ radiation. The crystal was mounted in a Cryoloop under Paratone-N oil and cooled to 110 K with an Oxford-Diffraction Cryojet. Data were collected using $\omega$ scans with 0.5° frame widths to a resolution of 0.75 Å, equivalent to $2\theta \approx 56.23°$. Reflections were recorded, indexed, and corrected for absorption using the Oxford-Diffraction CrysAlisPro software,[24] and subsequent structure determination and refinement was carried out using CRYSTALS,[25] employing Sir92[27] to solve the crystal structure. The refinement was performed against $F^2$, with anisotropic thermal displacement parameters for all inorganic framework atoms.

Considering the inorganic clusters comprising the framework of the structure and omitting any organic ligands would indicate a nearly centrosymmetric arrangement of the atoms with space group symmetry $P6_3/mmc$. However, this symmetry is too high to place solvent molecules into the structure and was therefore rejected. A number of lower symmetry space group possibilities were explored, but as in the case of the related structure (bmpy)$_9$[ZnCl$_4$]$_2$[Pb$_3$Cl$_{11}$] (CCDC 1913725),[16] we found that lower symmetries (monoclinic and triclinic) did not yield any further insight into the organic ligand positions and that higher symmetries must be rejected because of short organic ligand contacts. These findings led us to concentrate on the symmetry $P6_3$ to best describe the (bmpy)$_9$[ZnBr$_4$]$_2$[Pb$_3$Br$_{11}$] structure.

The inorganic clusters of the structure, the Pb$_3$Br$_{11}$ trimer and the ZnBr$_4$ inorganic clusters, were easily identified and refined without constraints. Subsequently, fragments of the organic ligands were identified using an electron density difference map. The molecular fragments were completed and incorporated into the model according to an ideal molecular configuration as determined in a previous structural refinement, CCDC deposition 1895392. The isotropic thermal displacements of all atoms comprising these ligands were then fixed to 0.2 Å$^2$, and the atomic positions were refined. In order to preserve a physically realistic model, the bonding distances and angles of atoms within the organic ligands were restrained to within ~5% when compared with the ideal geometry. Finally, all hydrogens were geometrically placed and constrained to their respective carbon atoms. The ligands placed in this way fit well into the structure of the inorganic framework; thus, the space group symmetry $P6_3$ was retained to describe the overall structure.

Although the organic ligands 1-butyl-1-methylpyrrolidinium provide a large fraction of the overall electron density, they do not yield strong enough scattering data to allow for unconstrained refinement; there remains some ambiguity in the exact details of the organic ligand conformation as obtained from our SCXRD measurements. However, the model presented shows the general location and orientation of the organic ligands based on the observed electron density.

**Powder X-ray Diffraction.** The powder X-ray diffraction (PXRD) analysis was performed on Panalytical X'PERT Pro diffractometer, equipped with an X'Celerator RTMS detector and copper K$\alpha$ radiation, at a voltage of 40 kV and a current of 40 mA. The diffraction pattern was scanned over the angular range of 5−50° ($2\theta$) with a step size of 0.02° at room temperature. Simulated powder patterns were calculated by Mercury software using the crystallographic information file from SCXRD experiment.

**Thermogravimetry Analysis.** TGA was carried out using a TA instruments Q600 SDT system. The samples were heated from room temperature (~22 °C) to 800 °C at a rate of 5 °C·min$^{-1}$, under an argon flux of 40 mL·min$^{-1}$.

**Absorption Spectrum Measurements.** Absorption spectra of (bmpy)$_6$Pb$_3$Br$_{12}$ and (bmpy)$_9$[ZnBr$_4$]$_2$[Pb$_3$Br$_{11}$] were measured at room temperature through a synchronous scan in an integrating sphere incorporated into the spectrofluorometer (FLS980, Edinburgh Instruments) while maintaining a 1 nm interval between the excitation and emission monochromators.

**Excitation Spectrum Measurements.** Excitation spectra of (bmpy)$_6$Pb$_3$Br$_{12}$ and (bmpy)$_9$[ZnBr$_4$]$_2$[Pb$_3$Br$_{11}$] were measured at room temperature and at 77 K (liquid nitrogen was used to cool the samples) on a FS5 spectrofluorometer (Edinburgh Instruments) monitored at maximum emission spectra.

**Photoluminescence Steady-State Studies.** Steady-state PL spectra of (bmpy)$_6$Pb$_3$Br$_{12}$ and (bmpy)$_9$[ZnBr$_4$]$_2$[Pb$_3$Br$_{11}$] were obtained at room temperature and at 77 K (liquid nitrogen was used to cool the samples) on a FS5 spectrofluorometer.

**Temperature-Dependent Photoluminescence from 80 K to RT.** Measurements of PL at different temperatures were performed on the crystals sandwiched between glass microscope slides (1 × 2.5 cm). Samples were held inside an OptistatDN variable liquid nitrogen cryostat (Oxford Instruments) at a 45° angle to the excitation source by a 2 cm × 2 cm sample holder fixed to the end of a cryostat sample holder. The emission spectra were collected at 90° to the excitation source with a Photon Technology International spectrophotometer with a photomultiplier detection system. The monochromatic excitation at $\lambda$ = 345 nm was used. Individual spectra were recorded at intervals of 10 K with the aid of an Omega CYC3200 auto-tuning temperature controller and a thermocouple wire affixed to the sample glass slide. Dry nitrogen was passed through the sample compartment to avoid condensation on the outer cryostat windows.

**Temperature-Dependent Photoluminescence from RT to 353 K for (bmpy)$_9$[ZnBr$_4$]$_2$Pb$_3$Br$_{11}$.** The temperature-dependent PL spectra were measured on a Varian Cary Eclipse Fluorescence Spectrometer with a Water 4 Position Multicell Holder Accessory attached to a Julabo F12-EC Refrigerated/Heating Circulator filled with ethylene glycol−water mixture (3:2).

**Photoluminescence Intensity Dependence on Excitation Power Density.** The power-dependent PL intensity measurements were carried out on an Edinburgh Instruments PL980-KS transient absorption spectrometer using a Continuum Nd:YAG laser (Surelite EX) pumping a Continuum optical parametric oscillator (Horizon II OPO) to provide 360 nm 5 ns pulses at 1 Hz. The pump beam profile was carefully defined using collimated laser pulses passed through an iris set to an area of 0.13 cm$^2$. The pulse intensity was monitored by a power meter (Ophir PE10BF-C), detecting the reflection from a beam splitter. Detection consisted of an Andor Intensified CCD (1024 × 256 element) camera, collecting a spectrum from 287 to 868 nm and gated to optimize PL collection(typically a 30−50 ns gate depending on the PL lifetime, starting immediately following the 5 ns laser pulse). Twenty collections were averaged at each power level with every laser pulse monitored to determine the average intensity. The PL was determined at the maximum of the PL emission curve.

**Photoluminescence Quantum Efficiencies.** The PLQEs were obtained using a Hamamatsu Quantaurus-QY Spectrometer (model C11347-11) equipped with a xenon lamp, integrated sphere sample chamber, and CCD detector. The PLQEs were calculated by using the equation: $\eta_{QE} = I_S/(E_R - E_S)$, in which $I_S$ represents the luminescence emission spectrum of the sample, $E_R$ is the spectrum of the excitation light from the empty integrated sphere (without the sample), and $E_S$ is the excitation spectrum for exciting the sample.

**Time-Resolved Photoluminescence.** Time-resolved emission data were carried out at room temperature using the FLS980 spectrofluorometer. The dynamics of emission decay were monitored by using the FLS980's time-correlated single-photon counting capability (1024 channels; 10 $\mu$s window) with data collection for 10 000 counts. Excitation was provided by an Edinburgh EPL-360 picosecond pulsed diode laser. Long lifetime measurements at 77 K (1024 channels; 800 $\mu$s window) were collected using a Xe flash lamp as the excitation source. The average lifetime was obtained by exponential fitting.

## ■ ASSOCIATED CONTENT

### Supporting Information

The Supporting Information is available free of charge at https://pubs.acs.org/doi/10.1021/acs.chemmater.9b03893.

Characterizations and analyses of the structural and photophysical properties of bulk assemblies of metal halide clusters (PDF)

Crystallographic data for **T1** (CIF)

Crystallographic data for **T2** (CIF)

## ■ AUTHOR INFORMATION

### Corresponding Author

*E-mail: bma@fsu.edu.

### ORCID

Chenkun Zhou: 0000-0001-9388-7517

Biwu Ma: 0000-0003-1573-8019

### Notes

The authors declare no competing financial interest.

## ■ ACKNOWLEDGMENTS

This work is supported by the National Science Foundation (DMR-1709116) and the Air Force Office of Scientific Research (AFOSR) (17RT0906). J.N. acknowledges support from NSF-DMR-1606952. Part of the work was carried out at the National High Magnetic Field Laboratory, which is supported by the National Science Foundation under NSF DMR-1644779 and the State of Florida. The authors thank Dr. Kenneth Hanson for the help with emission measurements.

## ■ REFERENCES

(1) Dou, L.; Yang, Y. M.; You, J.; Hong, Z.; Chang, W. H.; Li, G.; Yang, Y. Solution-processed hybrid perovskite photodetectors with high detectivity. *Nat. Commun.* **2014**, *5*, 5404.

(2) Yang, W. S.; Park, B.-W.; Jung, E. H.; Jeon, N. J.; Kim, Y. C.; Lee, D. U.; Shin, S. S.; Seo, J.; Kim, E. K.; Noh, J. H.; Seok, S. I. Iodide management in formamidinium-lead-halide–based perovskite layers for efficient solar cells. *Science* **2017**, *356*, 1376–1379.

(3) Heo, J. H.; Lee, D. S.; Shin, D. H.; Im, S. H. Recent advancements in and perspectives on flexible hybrid perovskite solar cells. *J. Mater. Chem. A* **2019**, *7*, 888–900.

(4) Stranks, S. D.; Snaith, H. J. Metal-halide perovskites for photovoltaic and light-emitting devices. *Nat. Nanotechnol.* **2015**, *10*, 391–402.

(5) Zhao, B.; Bai, S.; Kim, V.; Lamboll, R.; Shivanna, R.; Auras, F.; Richter, J. M.; Yang, L.; Dai, L.; Alsari, M.; She, X.-J.; Liang, L.; Zhang, J.; Lilliu, S.; Gao, P.; Snaith, H. J.; Wang, J.; Greenham, N. C.; Friend, R. H.; Di, D. High-efficiency perovskite–polymer bulk heterostructure light-emitting diodes. *Nat. Photonics* **2018**, *12*, 783–789.

(6) Dou, L.; Wong, A. B.; Yu, Y.; Lai, M.; Kornienko, N.; Eaton, S. W.; Fu, A.; Bischak, C. G.; Ma, J.; Ding, T.; Ginsberg, N. S.; Wang, L.-W.; Alivisatos, A. P.; Yang, P. Atomically thin two-dimensional organic-inorganic hybrid perovskites. *Science* **2015**, *349*, 1518–1521.

(7) Smith, M. D.; Crace, E. J.; Jaffe, A.; Karunadasa, H. I. The Diversity of Layered Halide Perovskites. *Annu. Rev. Mater. Res.* **2018**, *48*, 111–136.

(8) Yuan, Z.; Zhou, C.; Tian, Y.; Shu, Y.; Messier, J.; Wang, J. C.; van de Burgt, L. J.; Kountouriotis, K.; Xin, Y.; Holt, E.; Schanze, K.; Clark, R.; Siegrist, T.; Ma, B. One-dimensional organic lead halide perovskites with efficient bluish white-light emission. *Nat. Commun.* **2017**, *8*, 14051.

(9) Lin, H.; Zhou, C.; Neu, J.; Zhou, Y.; Han, D.; Chen, S.; Worku, M.; Chaaban, M.; Lee, S.; Berkwits, E.; Siegrist, T.; Du, M. H.; Ma, B. Bulk Assembly of Corrugated 1D Metal Halides with Broadband Yellow Emission. *Adv. Opt. Mater.* **2019**, *7*, 1801474.

(10) Zhou, C.; Lin, H.; Tian, Y.; Yuan, Z.; Clark, R.; Chen, B.; van de Burgt, L. J.; Wang, J. C.; Zhou, Y.; Hanson, K.; Meisner, Q. J.; Neu, J.; Besara, T.; Siegrist, T.; Lambers, E.; Djurovich, P.; Ma, B. Luminescent zero-dimensional organic metal halide hybrids with near-unity quantum efficiency. *Chem. Sci.* **2018**, *9*, 586–593.

(11) Zhou, C.; Lin, H.; He, Q.; Xu, L.; Worku, M.; Chaaban, M.; Lee, S.; Shi, X.; Du, M.-H.; Ma, B. Low dimensional metal halide perovskites and hybrids. *Mater. Sci. Eng., R* **2019**, *137*, 38–65.

(12) Zhou, C.; Lin, H.; Shi, H.; Tian, Y.; Pak, C.; Shatruk, M.; Zhou, Y.; Djurovich, P.; Du, M.-H.; Ma, B. A Zero-Dimensional Organic Seesaw-Shaped Tin Bromide with Highly Efficient Strongly Stokes-Shifted Deep-Red Emission. *Angew. Chem., Int. Ed.* **2018**, *57*, 1021.

(13) Zhou, C.; Lin, H.; Shi, H.; Tian, Y.; Pak, C.; Shatruk, M.; Zhou, Y.; Djurovich, P.; Du, M.-H.; Ma, B. A Zero-Dimensional Organic Seesaw-Shaped Tin Bromide with Highly Efficient Strongly Stokes-Shifted Deep-Red Emission. *Angew. Chem., Int. Ed. Engl.* **2018**, *57*, 1021–1024.

(14) Xu, L. J.; Sun, C. Z.; Xiao, H.; Wu, Y.; Chen, Z. N. Green-Light-Emitting Diodes based on Tetrabromide Manganese(II) Complex through Solution Process. *Adv. Mater.* **2017**, *29*, 1605739.

(15) Zhou, C.; Lin, H.; Worku, M.; Neu, J.; Zhou, Y.; Tian, Y.; Lee, S.; Djurovich, P.; Siegrist, T.; Ma, B. Blue Emitting Single Crystalline Assembly of Metal Halide Clusters. *J. Am. Chem. Soc.* **2018**, *140*, 13181–13184.

(16) Zhou, C.; Lin, H.; Neu, J.; Zhou, Y.; Chaaban, M.; Lee, S.; Worku, M.; Chen, B.; Clark, R.; Cheng, W.; Guan, J.; Djurovich, P.; Zhang, D.; Lü, X.; Bullock, J.; Pak, C.; Shatruk, M.; Du, M.-H.; Siegrist, T.; Ma, B. Green Emitting Single-Crystalline Bulk Assembly of Metal Halide Clusters with Near-Unity Photoluminescence Quantum Efficiency. *ACS Energy Lett.* **2019**, *4*, 1579–1583.

(17) Smith, M. D.; Watson, B. L.; Dauskardt, R. H.; Karunadasa, H. I. Broadband Emission with a Massive Stokes Shift from Sulfonium Pb–Br Hybrids. *Chem. Mater.* **2017**, *29*, 7083–7087.

(18) Pan, J.; Sun, A.-H.; Han, S.-D.; Wei, L.; Li, J.-H.; Wang, G.-M. Low-Dimensional Lead(II) Halides with In Situ Generated Tripyridine-Derivatives as Countercations: Synthesis, Structures and Properties. *J. Cluster Sci.* **2017**, *28*, 2669–2679.

(19) Thirumurugan, A.; Rao, C. N. R. Supramolecular Organization in Lead Bromide Salts of Imidazolium-Based Ionic Liquids. *Cryst. Growth Des.* **2008**, *8*, 1640–1644.

(20) Zhou, J.; Li, M.; Ning, L.; Zhang, R.; Molokeev, M. S.; Zhao, J.; Yang, S.; Han, K.; Xia, Z. Broad-Band Emission in a Zero-Dimensional Hybrid Organic [$PbBr_6$] Trimer with Intrinsic Vacancies. *J. Phys. Chem. Lett.* **2019**, *10*, 1337–1341.

(21) Wang, C.-H.; Du, H.-J.; Li, Y.; Niu, Y.-Y.; Hou, H.-W. Crystal structures and photocatalytic properties of two novel iodoplumbate hybrids templated by multivalent organic cations. *New J. Chem.* **2015**, *39*, 7372–7378.

(22) Shen, J.-J.; Wang, F.; Yu, T.-L.; Zhang, F.-Q.; Tian, L.; Fu, Y.-L. Halogen-dependent photoinduced electron transfer and chromism of three protonated nicotinohydrazide halozincates. *Dalton Trans.* **2017**, *46*, 5414–5419.

(23) Zhou, C.; Tian, Y.; Yuan, Z.; Han, M.; Wang, J.; Zhu, L.; Tameh, M. S.; Huang, C.; Ma, B. Precise Design of Phosphorescent Molecular Butterflies with Tunable Photoinduced Structural Change and Dual Emission. *Angew. Chem., Int. Ed. Engl.* **2015**, *54*, 9591–9595.

(24) Diffraction, R. O. *CrysAlisPro Software System*, Version 1.171.38.43; Rigaku Corporation, 2016.

(25) Betteridge, P. W.; Carruthers, J. R.; Cooper, R. I.; Prout, K.; Watkin, D. J. CRYSTALS version 12: software for guided crystal structure analysis. *J. Appl. Crystallogr.* **2003**, *36*, 1487.

(26) Palatinus, L.; Chapuis, G. SUPERFLIP– a computer program for the solution of crystal structures by charge flipping in arbitrary dimensions. *J. Appl. Crystallogr.* **2007**, *40*, 786–790.

(27) Altomare, A.; Cascarano, G.; Giacovazzo, C.; Guagliardi, A.; Burla, M. C.; Polidori, G.; Camalli, M. SIRPOW.92 - a program for

automatic solution of crystal structures by direct methods optimized for powder data. *J. Appl. Crystallogr.* **1994**, 27, 435.